Cooperative, Nanoparticle-Enabled Thermal Therapy of Breast Cancer

Haifa Shen, Jian You, Guodong Zhang, Arturas Ziemys, Qingpo Li, Litao Bai, Xiaoyong Deng, Donald R. Erm, Xuewu Liu, Chun Li, and Mauro Ferrari**

Despite decades of research and drug development for cancer treatment, cancer still remains one of the major causes of human deaths in the world.[1] Human cancers consist of a mixed population of malignant cells that carry multiple genetic mutations. It has been estimated that there are around 40 DNA mutations that result in amino acid changes in an individual tumor of glioblastoma[2] or pancreatic cancer,[3] and twice as many mutations in breast and colorectal cancers.[4] Many of them are driver mutations that determine tumor initiation, progression, and metastasis. The genomic landscapes indicate that multiple signal transduction pathways determine the fate of a cancer cell, and it is almost impossible to treat cancer with a single therapeutic agent. It is thus not surprising that many of the recently developed targeted therapy drugs, such as the EGFR inhibitors for non-small-cell lung-cancer treatment and Herceptin for breast-cancer therapy, are effective in only a certain set of cancer patients;[5,6] and in many cases, drug resistance arises from additional genetic and epigenetic alterations. It has been reported that mutations within the EGFR gene,[7,8] the KRAS gene,[9,10] and up-regulation of other signaling pathways[11,12] could all cause resistance to EGFR-targeted therapy. Clearly, there is an urgent and persistent motivation to develop novel therapeutics independent of the genetic background of the cancer in the fight against this deadly disease.

Nanotechnology has played a crucial role in the development of cancer therapeutics.[13] Doxil and Abraxane[14–17] are just two examples of nanoformulated drugs. Gold nanoparticles (AuNPs) are currently being explored to induce hyperthermic cytotoxicity.[18–22] When exposed to light at the correct wavelength, the conduction-band electrons of the nanoparticle generate heat that is transmitted to the cells and surrounding tissues. Thermal therapy has the advantage of killing cancer cells without causing resistance regardless of the genetic background, and thus can be applied to all cancer patients. However, successful application of this approach requires adequate accumulation of AuNPs in the tumor and sufficient tumor penetration of the excitation energy.[23] Due to lack of effective delivery, tumor delivery of AuNPs in most studies has been relied on the enhanced permeability and retention (EPR) effect, a result of tumor blood vessel leakiness due to a state of ongoing angiogenesis, and thus has not been very efficient.[24] It has been reported that less than 5% of the total injected dose of PEGylated AuNPs could ultimately reach the tumor tissue.[22] The amount of AuNPs needed for each treatment makes it impractical for clinical therapies. Besides, AuNPs tend to accumulate unevenly in the tumor tissue dependent on particle size, surface charge, and other factors,[25–27] which makes it difficult to eradicate the whole tumor tissue with this approach.

We have previously developed a multistage vector delivery system based on porous silicon (pSi). This system is composed of two delivery carriers: the first stage is a degradable pSi vector and the second stage nanoparticles are loaded into the pores of pSi. The nanoparticles can be liposomes or micelles incorporated with therapeutics (third stage) or diagnostic agents.[28] A major advantage of this system is that the size, shape, and surface properties of pSi can be tailored so that maximal tissue-specific localization and release of the therapeutics at the target tumor can be achieved.[28–31] We have recently demonstrated successful application of this system to deliver siRNA therapeutics for cancer treatment with two mouse models of ovarian cancers.[32,33]

Here, we designed a pSi nanoassembly with hollow gold nanoshells (HAuNSs) to explore photothermal effects for therapeutics, taking advantage of the nanoscale effect. HAuNSs are favorable over solid AuNPs, since hollow gold responds to near-infrared (NIR) light, which has a deep penetration inside the body and causes less damage comparing to a shorter wavelength light to tissues due to less absorbance by the tissue chromophores. We used human and mouse breast cancer lines to test cell killing *in vitro* and the mouse model of 4T1 mammary tumor for *in vivo* studies. The potential mechanism of action with the new therapeutics will be discussed.

pSi particles were fabricated in three major steps: the formation of porous silicon films, photolithographic patterning of particles, and reactive ion etching. The porous structure of the particles was tailored by electrochemical etching to a mean pore size of 60 nm and a porosity of about 80%, while the particle sizes were precisely defined by photolithography to 1000 nm in diameter and 400 nm in thickness. Scanning electron microscopy (SEM) images revealed that the pores were evenly distributed across the whole area (**Figure 1**A and B). Since the surface

---

Prof. H. Shen, G. Zhang, Prof. A. Ziemys, Q. Li, L. Bai, X. Deng, Donald R. Erm, Prof. X. Liu, Prof. M. Ferrari
The Methodist Hospital Research Institute
Department of Nanomedicine
6670 Bertner Ave., Houston, Texas 77030
E-mail: hshen@tmhs.org; mferrari@tmhs.org
J. You, Prof. C. Li
The University of Texas M D Anderson Cancer Center
Department of Experimental Diagnostic Imaging
1515 Holcombe Blvd., Houston, Texas 77030

DOI: 10.1002/adhm.201100005

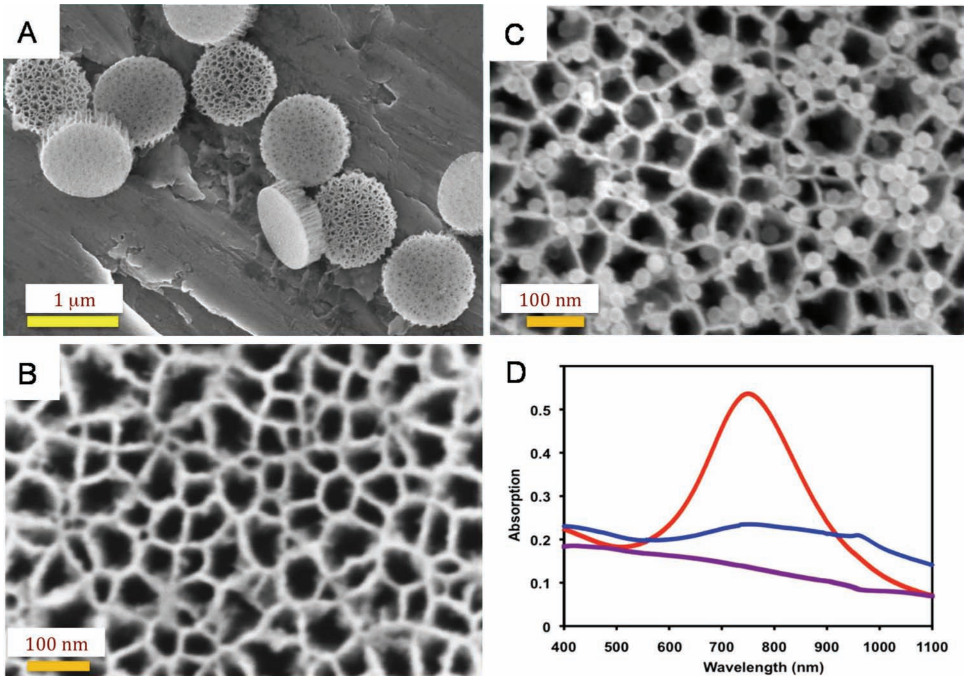

Figure 1. SEM images of empty pSi and pSi/HAuNSs. The SEM imaging of particles was performed using a ZEISS NEON 40 scanning electron microscope. To prepare the SEM samples, a drop of IPA particle suspension was directly placed on a clean aluminum SEM sample stub and dried. The samples were loaded into the SEM chamber, and SEM images were measured at 5 kV and 3–5 mm working distance using an in-lens detector. A,B) SEM images of monodispersed 1000 nm × 400 nm discoidal pSi particles with 60 nm mean pore size. C) SEM image of silicon particles loaded with HAuNSs. D) Absorption spectra of pSi (purple), HAuNSs (red), and pSi/HAuNSs (blue).

of the silicon particles was conjugated with 3-aminopropyltriethoxysilane (APTES), these particles were positively charged, which facilitated loading of the negatively charged HAuNSs by favorable electrostatic interactions (Figure 1C). Multiple HAuNSs particles could be found in each pore across the whole silicon microparticle.

We carried out a spectrum scan to determine absorption profiles. The HAuNS particles of 28 nm in diameter showed a plasma resonance peak at 750 nm (Figure 1D), which has previously been observed for most HAuNS particles of similar size.[34,35] This peak disappeared when the HAuNS particles were loaded into pSi. There was a small peak around 950 nm indicating a red shift of the absorbance from pSi/HAuNSs (Figure 1D), while empty pSi particles did not have any significant absorption in the 400–1100 nm range. We have also measured the absorption spectra of solid AuNPs with a plasma resonance peak at 528 nm (Supporting Information, Figure S1). Loading of AuNPs into pSi also resulted in the disappearance of the peak and a red shift of the small peak in the 600–750 nm range. Simply mixing AuNPs with silicon did not result in a disappearance of the plasma resonance peak (data not shown). The most plausible explanation for vanishing absorption from the pSi/HAuNSs nanoassembly is a scattering effect from the pSi microparticle.

A water suspension of the particles was used to measure the heat generation triggered by NIR laser irradiation. pSi particles alone did not show any heat generation, as expected, and constantly remained at room temperature during continous exposure to NIR laser irradiation (**Figure 2**). The temperature in the HAuNS colloidal suspension increased by 10.9 °C and reached a steady level of 34.7 °C within 10 min. A bigger increase in temperature was observed in the pSi/HAuNS suspension.

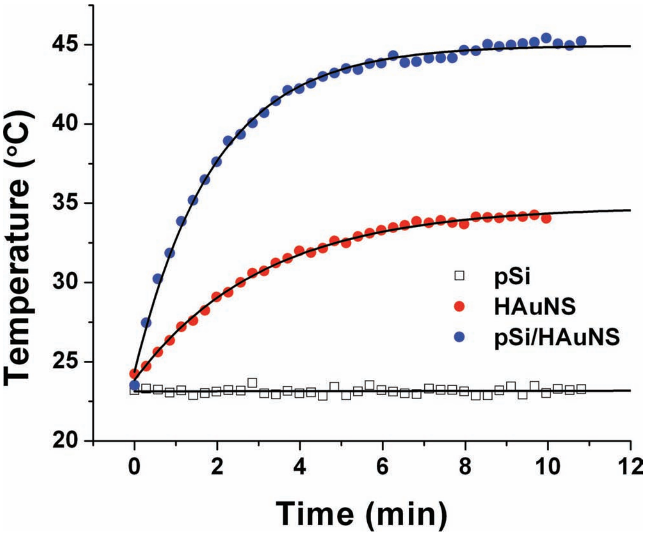

Figure 2. Heat-generation kinetics of free HAuNSs and pSi/HAuNSs. The temperature change was measured over a period of 10 min of exposure to NIR with a wavelength of 808 nm and an output power of 0.5 w. The same amount of HAuNS particles were used in the samples of free HAuNSs and pSi/HAuNSs. Equal amounts of unloaded pSi particles as in pSi/HAuNSs were used as a control samples. Experimental data are shown with the best exponential fit.

The temperature reached 45.0 °C within 7 min, an overall increase of 20.6 °C from room temperature, which corresponds to almost twice the temperature increase found for the same amount of colloidal HAuNSs. The time constants for heat generation kinetics were calculated at 3.1 s for HAuNSs and 1.9 s for pSi/HAuNSs.

To test whether the enhanced thermal generation could be translated into efficient cell killing, we treated cancer cells with free HAuNSs or pSi/HAuNSs and monitored cell growth using a MTT assay. pSi and AuNP were used as controls. The AuNP particles were not expected to have any effect on thermal cytotoxicity, as the NIR laser used in the study with a wavelength of 808 nm did not have any impact on the solid gold. We loaded different amount of HAuNSs into a fixed number of silicon particles (2×10^9 HAuNSs or 2×10^{10} HAuNSs in 1×10^8 pSi), so that any changes in cell growth would arise from the impact of HAuNSs, but not from silicon particles. As expected, neither free HAuNSs nor pSi/HAuNSs had any significant impact on cell growth if there was not enough HAuNSs for heat generation (**Figure 3**A). However, when the number of gold particles increased, the pSi/HAuNSs was very efficient in killing cancer cells, while the effect from free HAuNSs was mild (Figure 3A). Further increase of the HAuNS particle numbers resulted in cell killing from both free gold and the gold-silicon nanoassembly (data not shown). A similar trend was observed with MDA-MB-231 and SK-BR-3 human breast cancer cells (Figure 3A, upper and middle panels) and 4T1 murine mammary tumor cells (Figure 3A, bottom panel). These results indicate that the thermal ablation effect is general, since these cell lines carry significantly different genetic background and diverse mutation spectra. For example, the SK-BR-3 cells overexpress the HER2 gene, while MDA-MB-231 is a triple-negative cell line lacking the expression of estrogen receptor, progesterone receptor, and HER2.

We used two dyes to detect cell viability after exposure to NIR laser. The nonfluorescent calcein AM was converted to the intensely green fluorescent calcein in live cells. Ethidium

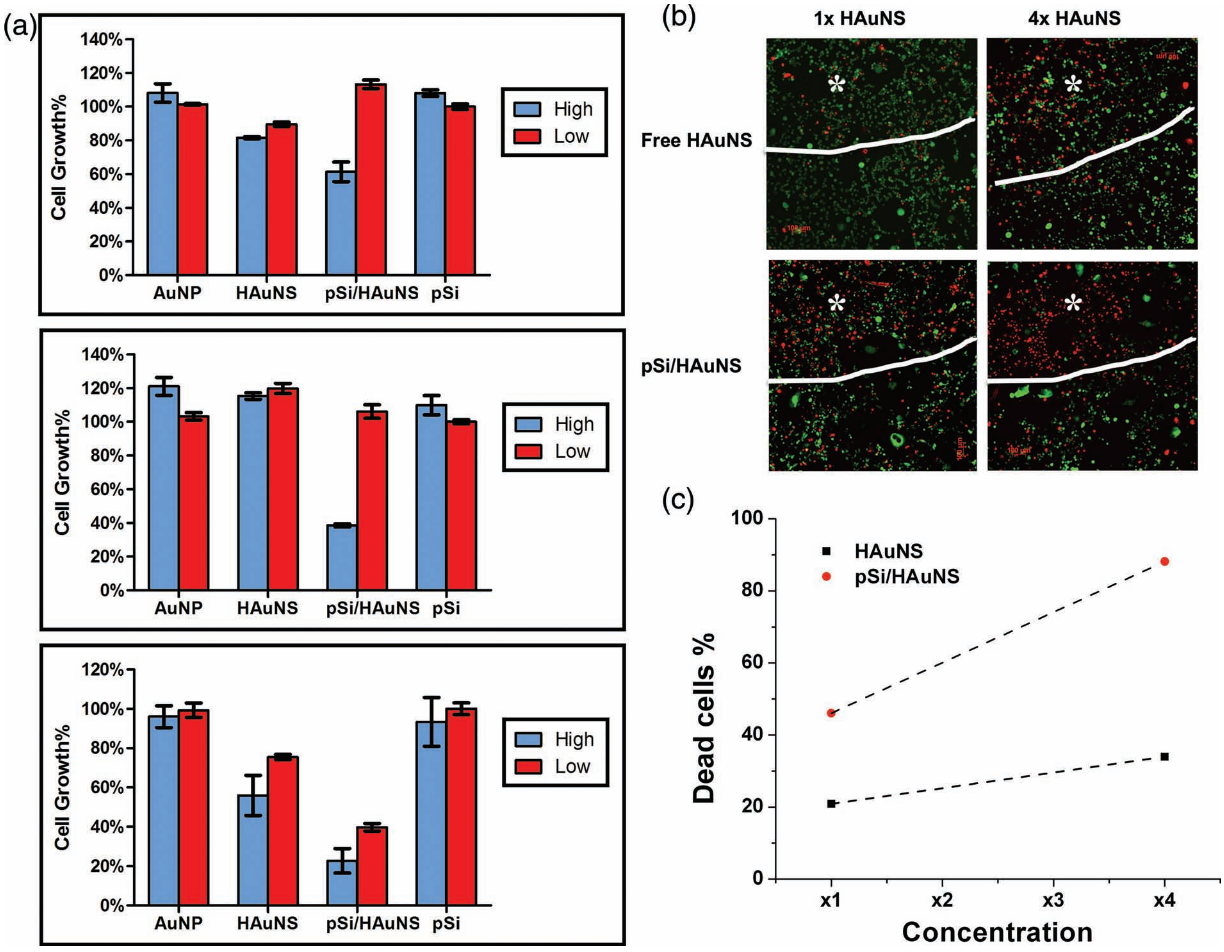

Figure 3. Photothermal effect on cancer cell growth in vitro and in vivo. a) Cell survival as a function of HAuNS concentration. Cancer cells were incubated with a high dose (2×10^{10} per well, in blue) and a low dose (2×10^9 per well, in red) of free AuNP, free HAuNSs, or pSi/HAuNSs, and treated with NIR. Cell survival was measured by the MTT assay. Percentage of cell growth was calculated by comparing the growth of treated cells to untreated control cells. Upper panel: MDA-MB-231 cells; middle panel: SK-BR-3 cells; bottom panel: 4T1 cells. b) Cell viability staining after NIR treatment of MDA-MB-231 cells incubated with free HAuNSs or pSi/HAuNSs. MDA-MB-231 cells were incubated with a low-dose (1X) or a high dose (4X) free HAuNSs or pSi/HAuNSs, and treated with NIR. Live cells were stained green with calcein AM, and dead cells were stained red with EthD-1. The boundary of NIR laser beam was marked with a white line in each well, and the area hit by laser was marked with an asterisk. c) Analysis of cell-staining result. Percentage of dead cells in each well was normalized with untreated control cells.

homodimer-1 (EthD-1) entered dead/dying cells through damaged membranes and bound to nucleic acid, producing a bright-red fluorescence. Cells were treated with a low dose (1×, 6.25×10^9 HAuNSs per well) and a high dose (4×, 2.5×10^{10} HAuNSs per well) free HAuNSs or pSi/HAuNSs. Around 20% cells were positive for EthD-1 staining without NIR laser treatment (Supporting Information, Figure 2). The free HAuNS-treated cells did not undergo significant cell death at the 1× dose (Figure 3B, upper left). The amount of EthD-1-positive cells doubled with the 4× HAuNS dose (Figure 3B, upper right); however, the percentage of dead cells was not as high as in the sample treated with the 1× dose pSi/HAuNSs (Figure 3B, upper right vs. bottom left). Up to 88% cancer cells treated with 4× pSi/HAuNSs were EthD-1-positive 24 h after NIR treatment, comparing to less than 35% EthD-1-positive cells treated with 4× HAuNSs (Figure 3B, bottom right). Quantitative analysis of cell death from these treatments is shown in Figure 3C. This result was in perfect agreement with the thermal generation result, which showed that the increase of temperature was three times as fast from the same amount of HAuNSs in the nanoassembly as from free HAuNSs. These results indicate that enhanced cancer-cell killing can be achieved through packaging AuNS into a pSi nanoassembly.

In a proof-of-principle study, we generated murine 4T1 tumor mice to test the efficacy of thermal ablation by pSi/HAuNSs on tumor growth. When the tumors reached sizes of 150–200 mm^3, free HAuNSs or pSi/HAuNSs were delivered by intratumor injection. The tumors were treated with NIR laser the next day, and tumor growth was monitor over the following 10 days before the mice were sacrificed. A single treatment of thermal ablation from both free HAuNSs and pSi/HAuNSs significantly inhibited tumor growth (**Figure 4**). However, the pSi/HAuNSs-treated mice did not have much tumor growth, while the tumor weight in the free HAuNSs group more than doubled during the same period of time. In the pSi control group, the average tumor weight almost quadrupled to 1 g per tumor. This result clearly supports the application of the pSi/HAuNSs assembly in cancer therapy.

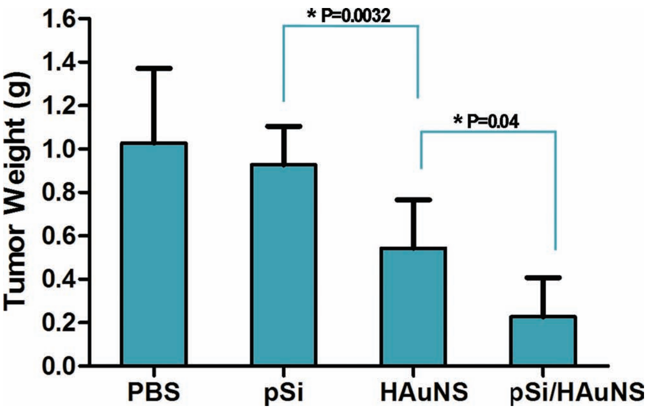

Figure 4. Photothermal therapy of murine 4T1 tumor. Mice were inoculated with 4T1 tumor cells and divided into four treatment groups ($n = 8$). When tumors reached an average size of 150–200 mm^3, the tumor mice were administrated with free HAuNSs or the same amount of HAuNSs in a pSi nanoassembly by intratumor injection and treated with NIR light. The PBS and pSi groups served as controls. The result is a summary of tumor weight 10 days after treatment.

Previous studied have demonstrated the potential application of pSi as a multistage vector for the delivery of therapeutics and imaging agents.[32,33,36] Due to the nature of the size and porosity, pSi can be used as a cargo to deliver a large quantity of therapeutic agents and can achieve tumoritropic accumulation independent of the EPR effect. In this study, pSi is used not only for enhanced tumor localization but also as an essential part of the therapeutic complex for the enhancement of thermal ablation, making it a part of therapeutic mechanism. We have analyzed the kinetics of heat generation by HAuNSs with respect to heat exchange. Theoretical models of AuNP suspensions have been developed,[37,38] where the energy balance was governed by laser-induced heat through electron–phonon relaxations on HAuNS surfaces and heat dissipation. The temperature profile generated by laser was derived by introducing the rate of energy adsorption, A [K s^{-1}], and the rate of heat loss, B [s^{-1}][37]:

$$T(t) = T_0 + \frac{A}{B}(1 - \exp(-Bt)) \tag{1}$$

We have fitted Equation 1 to the temperature profiles in Figure 2, where $A = 4.17$ K s^{-1} and B = 0.36 s^{-1} for HAuNSs and $A = 12.26$ K s^{-1} and $B = 0.56$ s^{-1} for pSi/HAuNSs. The rate of heat generations was three times as high for pSi/HAuNSs as for free HAuNSs. We had anticipated that both HAuNSs and pSi/HAuNSs would have similar heat loss rates, since the only difference was the inclusion of pSi in the nanoassembly. Interestingly, the heat dissipation rate was also higher for the pSi/HAuNSs nanoassembly. Thus, the model in Equation 1 that was validated for colloidal gold could not explain the pSi/HAuNSs temperature increase curve using the same heat-loss rates. This suggests that the thermal equilibrium of pSi/HAuNSs is defined by different thermal properties of the system.

The clear difference between HAuNSs and pSi/HAuNSs was the distribution of the AuNPs, which is summarized in **Figure 5**. Based on the amount of HAuNSs and pSi used in this study, we concluded that the average gold interparticle distance in colloidal HAuNSs was 1.7 μm, and free pSi particles were separated by 11 μm. In the pSi/HAuNSs nanoassembly, however, HAuNSs were fixed within pSi with a domain of less than 1 μm (Figure 1). It has been reported that surface plasmons penetrate dielectric media up to hundreds of nanometers away from metal surface[39,40] and that the specific orientation of HAuNSs can transfer energy over hundreds of nanometers.[41] Thus, HAuNS particles within the nanoassembly should become electromagnetically coupled mostly through dipole–dipole interactions[42] and can function as waveguide-like structures that increase energy transfer and heat production, as illustrated in Figure 5. To support our finding, increased heat production in HAuNS structures through varying the angle of an incident photon beam has already been observed.[43] Furthermore, bringing HAuNSs closer to clusters can cause a red shift of the surface-polaron resonance[44] that could be larger than 100 nm.[40] The peak around 950 nm found in pSi/HAuNSs, which was not observed in free HAuNSs suspension, indicates a red shift of 200 nm. The increased wavelength in the NIR region could be used for deeper penetration into tissues, where HAuNSs are arranged in a collective nanoscale structure. Potentially, an enhanced heating effect can also be supplemented by scattering, which increases the light path.

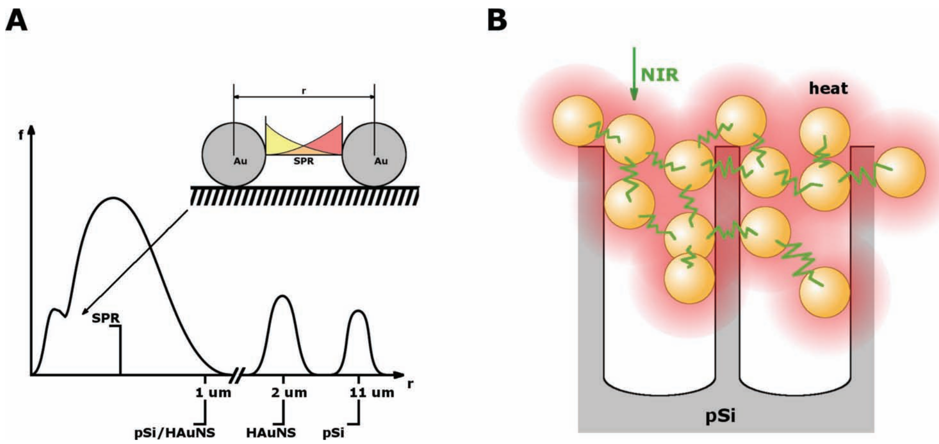

Figure 5. Potential mechanism of increased thermal efficiency from pSi/HAuNSs. A) Characteristic interparticle distances in our experiments for pSi, HAuNSs, and pSi/HAuNSs. HAuNSs and surface polaron interaction distances overlap enabling HAuNSs electromagnetic coupling within pSi, which is not possible for free HAuNSs. B) Proposed schematics of collective electromagnetic coupling of HAuNSs in pSi leading to a coherent thermal domain.

Since convective flows inside pSi are negligible, thermal diffusion is the most important aspect. Characteristic thermal diffusion lengths of water, expressed as $L_T = \sqrt{4Dt}$ over given time t and the thermal diffusivity $D = 1.4 \times 10^{-3}$ cm^2 s^{-1}, are 0.7 µm for 1 µs and 23.4 µm for 1 ms pulses. Therefore, using sub-microsecond-range NIR pulses, thermal expansion domains around individual HAuNSs will start to overlap, while NIR pulses over 1 µs will make pSi/HAuNSs a continuous thermally excited domain (thermal spot-source). Silicon has athermal diffusivity that is almost six times as high as that of water. At 80% porosity in pSi, the effective thermal diffusivity is 3.3×10^{-3} cm^2 s^{-1}. It has already been shown that thermal dissipation of AuNPs can be increased by wrapping the gold core with a silica shell.[45] Therefore, L_T of pSi increases by almost 50%, which makes heat dissipation even more efficient within premises of pSi, suggesting that the induced photothermal effects can be enhanced by thermal properties of the HAuNS organizing materials.

Our results have clearly shown the superior photothermal ablation effect from pSi/HAuNSs. We have demonstrated that the pSi/HAuNSs nanoassembly is much more efficient at heat generation than free AuNPs. Moreover, the nanoassembly offers the benefit of a red shift to access deeper tissues and more efficient energy-to-heat conversion. These properties are enabled through exploiting nanoscale organization features of HAuNSs and are demonstrated for the first time with therapeutic purposes.

Experimental Section

Fabrication of Discoidal pSi Particles and Surface Chemical Modifications: Discoidal pSi particles were fabricated as previously described.[36] The dried particles were then treated with piranha solution to obtain oxidized, negatively charged silicon particles and modified with 2% (v/v) APTES (Sigma–Aldrich, St. Louis, MO) for 24–36 h at 55 °C to obtain positively charged particles to load the nanoparticles. The synthesis of HAuNS was reported previously.[34,35] HAuNS were loaded into pSi by a combination of capillary force and surface charges.

Photothermal Effect in Aqueous Solution: The GCSLX-05-1600m-1 fiber-coupled diode laser (DHC, China Daheng Group, Beijing, P. R. China) with a center wavelength of 808 ± 10 nm was powered by a DH 1715A-5 dual-regulated power supply. A 5-m, 600-µm-core BioTex LCM-001 optical fiber (BioTex Inc., Houston, TX) was used to transfer laser power from the laser unit to the target. The end of the optical fiber was attached to a retort stand using a movable clamp and positioned directly above the sample cell. For measurement of temperature changes, NIR laser light was delivered through a quartz cuvette containing pSi, HAuNSs, or pSi/HAuNSs (100 µL). A thermocouple was inserted into the solution perpendicular to the path of the laser light. The temperature was measured over 10 min.

Photothermal Cytotoxicity In Vitro: Cancer cells were seeded into a 96-well plate at a density of 10 000 cells per well. Free HAuNSs or pSi/HAuNsS were added into the cell culture 5 h later, when the cell had attached to the plate. The cells were washed three times with serum-free media the next day and were irradiated with NIR light at an output power of 2 W for 2 min (for SK-BR-3 cells), or 3 min (for MDA-MB-231 and 4T1 cells). Cells were washed three times with Hank's balanced salt solution 24 h after the laser treatment and stained with the live/dead viability/cytotoxicity kit from Invitrogen according to the manufacturer suggested protocol. Live cells were stained with calcein acetoxymethyl ester and dead cells were stained with ethidium homodimer. Cells were examined using an Olympus Fluoview FV1000 confocal laser scanning microscope (FV1-ASW) equipped with filter sets specific for excitation/emission wavelengths at 494/517 nm for live cells (stained in green) and 528/617 nm for dead cells (stained in red).

Photothermal Therapy of Mammary Tumors in Nude Mice: Six-week-old nude mice were inoculated with 4T1 cells in the mammary gland fat pad. When the tumors reached 150–200 mm^3, the mice were administered with PBS, pSi, HAuNSs, or pSi/HAuNSs by intratumor injection. Each mouse in the treatment group received 3×10^8 pSi containing 1×10^{11} HAuNSs in 25 µL PBS. In the control groups, each mouse received 25 µL PBS, 3×10^8 empty pSi, or 1×10^{11} free HAuNS. The mice were treated with NIR light at 0.5 W for 3 min per tumor, and the tumor growth was monitored over the next two weeks. All animals were sacrificed when the tumor sizes in the PBS control group passed 1 000 mm^3.

Supporting Information

Supporting Information is available from the Wiley Online Library or from the author.

Acknowledgements

H.S. and J.Y. contributed equally to this work. The authors acknowledge financial supports from the following sources: Department of Defense grant DODW81XWH-09-1-0212, National Institute of Health grants NIH RO1CA128797, NIH–R33 CA122864, and NIH U54CA143837.

Received: July 14, 2011
Revised: September 16, 2011
Published online: November 29, 2011

[1] A. Jemal, R. Siegel, J. Xu,E. Ward, *CA Cancer J. Clin.* **2010**, *60*, 277.

[2] D. W. Parsons, S. Jones, X. Zhang, J. C. Lin, R. J. Leary, P. Angenendt, P. Mankoo, H. Carter, I. M. Siu, G. L. Gallia, A. Olivi, R. McLendon, B. A. Rasheed, S. Keir, T. Nikolskaya, Y. Nikolsky, D. A. Busam, H. Tekleab, L. A. Diaz Jr., J. Hartigan, D. R. Smith, R. L. Strausberg, S. K. Marie, S. M. Shinjo, H. Yan, G. J. Riggins, D. D. Bigner, R. Karchin, N. Papadopoulos, G. Parmigiani, B. Vogelstein, V. E. Velculescu, K. W. Kinzler, *Science* **2008**, *321*, 1807.

[3] S. Jones, X. Zhang, D. W. Parsons, J. C. Lin, R. J. Leary, P. Angenendt, P. Mankoo, H. Carter, H. Kamiyama, A. Jimeno, S. M. Hong, B. Fu, M. T. Lin, E. S. Calhoun, M. Kamiyama, K. Walter, T. Nikolskaya, Y. Nikolsky, J. Hartigan, D. R. Smith, M. Hidalgo, S. D. Leach, A. P. Klein, E. M. Jaffee, M. Goggins, A. Maitra, C. Iacobuzio-Donahue, J. R. Eshleman, S. E. Kern, R. H. Hruban, R. Karchin, N. Papadopoulos, G. Parmigiani, B. Vogelstein, V. E. Velculescu, K. W. Kinzler, *Science* **2008**, *321*, 1801.

[4] L. D. Wood, D. W. Parsons, S. Jones, J. Lin, T. Sjoblom, R. J. Leary, D. Shen, S. M. Boca, T. Barber, J. Ptak, N. Silliman, S. Szabo, Z. Dezso, V. Ustyankskу, T. Nikolskaya, Y. Nikolsky, R. Karchin, P. A. Wilson, J. S. Kaminker, Z. Zhang, R. Croshaw, J. Willis, D. Dawson, M. Shipitsin, J. K. Willson, S. Sukumar, K. Polyak, B. H. Park, C. L. Pethiyagoda, P. V. Pant, D. G. Ballinger, A. B. Sparks, J. Hartigan, D. R. Smith, E. Suh, N. Papadopoulos, P. Buckhaults, S. D. Markowitz, G. Parmigiani, K. W. Kinzler, V. E. Velculescu, B. Vogelstein, *Science* **2007**, *318*, 1108.

[5] T. J. Lynch, D. W. Bell, R. Sordella, S. Gurubhagavatula, R. A. Okimoto, B. W. Brannigan, P. L. Harris, S. M. Haserlat, J. G. Supko, F. G. Haluska, D. N. Louis, D. C. Christiani, J. Settleman, D. A. Haber, *N. Engl. J. Med.* **2004**, *350*, 2129.

[6] J. G. Paez, P. A. Janne, J. C. Lee, S. Tracy, H. Greulich, S. Gabriel, P. Herman, F. J. Kaye, N. Lindeman, T. J. Boggon, K. Naoki, H. Sasaki, Y. Fujii, M. J. Eck, W. R. Sellers, B. E. Johnson, M. Meyerson, *Science* **2004**, *304*, 1497.

[7] M. N. Balak, Y. Gong, G. J. Riely, R. Somwar, A. R. Li, M. F. Zakowski, A. Chiang, G. Yang, O. Ouerfelli, M. G. Kris, M. Ladanyi, V. A. Miller, W. Pao, *Clin. Cancer Res.* **2006**, *12*, 6494.

[8] S. Kobayashi, T. J. Boggon, T. Dayaram, P. A. Janne, O. Kocher, M. Meyerson, B. E. Johnson, M. J. Eck, D. G. Tenen, B. Halmos, *N. Engl. J. Med.* **2005**, *352*, 786.

[9] W. Pao, T. Y. Wang, G. J. Riely, V. A. Miller, Q. Pan, M. Ladanyi, M. F. Zakowski, R. T. Heelan, M. G. Kris, H. E. Varmus, *PLoS Med.* **2005**, *2*, e17.

[10] D. A. Eberhard, B. E. Johnson, L. C. Amler, A. D. Goddard, S. L. Heldens, R. S. Herbst, W. L. Ince, P. A. Janne, T. Januario, D. H. Johnson, P. Klein, V. A. Miller, M. A. Ostland, D. A. Ramies, D. Sebisanovic, J. A. Stinson,Y. R. Zhang, S. Seshagiri,K. J. Hillan, *J. Clin. Oncol.* **2005**, *23*, 5900.

[11] J. A. Engelman, K. Zejnullahu, T. Mitsudomi, Y. Song, C. Hyland, J. O. Park, N. Lindeman, C. M. Gale, X. Zhao, J. Christensen, T. Kosaka, A. J. Holmes, A. M. Rogers, F. Cappuzzo, T. Mok, C. Lee, B. E. Johnson, L. C. Cantley, P. A. Janne, *Science* **2007**, *316*, 1039.

[12] J. Bean, C. Brennan, J. Y. Shih, G. Riely, A. Viale, L. Wang, D. Chitale, N. Motoi, J. Szoke, S. Broderick, M. Balak, W. C. Chang, C. J. Yu, A. Gazdar, H. Pass, V. Rusch, W. Gerald, S. F. Huang, P. C. Yang, V. Miller, M. Ladanyi, C. H. Yang, W. Pao, *Proc. Natl. Acad. Sci. USA* **2007**, *104*, 20932.

[13] M. Ferrari, *Nat. Rev. Cancer* **2005**, *5*, 161.

[14] A. Rahman, J. Treat, J. K. Roh, L. A. Potkul, W. G. Alvord, D. Forst, P. V. Woolley, *J. Clin. Oncol.* **1990**, *8*, 1093.

[15] J. Treat, A. Greenspan, D. Forst, J. A. Sanchez, V. J. Ferrans, L. A. Potkul, P. V. Woolley, A. Rahman, *J. Natl. Cancer Inst.* **1990**, *82*, 1706.

[16] N. K. Ibrahim, B. Samuels, R. Page, D. Doval, K. M. Patel, S. C. Rao, M. K. Nair, P. Bhar, N. Desai, G. N. Hortobagyi, *J. Clin. Oncol.* **2005**, *23*, 6019.

[17] W. J. Gradishar, S. Tjulandin, N. Davidson, H. Shaw, N. Desai, P. Bhar, M. Hawkins, J. O'Shaughnessy, *J. Clin. Oncol.* **2005**, *23*, 7794.

[18] L. R. Hirsch, R. J. Stafford, J. A. Bankson, S. R. Sershen, B. Rivera, R. E. Price, J. D. Hazle, N. J. Halas, J. L. West, *Proc. Natl. Acad. Sci. USA* **2003**, *100*, 13549.

[19] E. S. Glazer, S. A. Curley, *Cancer* **2010**, *116*, 3285.

[20] D. P. O'Neal, L. R. Hirsch, N. J. Halas, J. D. Payne, J. L. West, *Cancer Lett.* **2004**, *209*, 171.

[21] J. A. Schwartz, A. M. Shetty, R. E. Price, R. J. Stafford, J. C. Wang, R. K. Uthamanthil, K. Pham, R. J. McNichols, C. L. Coleman, J. D. Payne, *Cancer Res.* **2009**, *69*, 1659.

[22] E. B. Dickerson, E. C. Dreaden, X. Huang, I. H. El-Sayed, H. Chu, S. Pushpanketh, J. F. McDonald, M. A. El-Sayed, *Cancer Lett.* **2008**, *269*, 57.

[23] L. C. Kennedy, L. R. Bickford, N. A. Lewinski, A. J. Coughlin, Y. Hu, E. S. Day, J. L. West, R. A. Drezek, *Small* **2011**, *7*, 169.

[24] H. Maeda, *Adv. Enzyme Regul.* **2001**, *41*, 189.

[25] P. Puvanakrishnan, J. Park, P. Diagaradjane, J. A. Schwartz, C. L. Coleman, K. L. Gill-Sharp, K. L. Sang, J. D. Payne, S. Krishnan, J. W. Tunnell, *J. Biomed. Opt.* **2009**, *14*, 024044.

[26] S. D. Perrault, C. Walkey, T. Jennings, H. C. Fischer, W. C. Chan, *Nano Lett.* **2009**, *9*, 1909.

[27] B. Kim, G. Han, B. J. Toley, C. K. Kim, V. M. Rotello, N. S. Forbes, *Nat. Nanotechnol.* **2010**, *5*, 465.

[28] E. Tasciotti, X. Liu, R. Bhavane, K. Plant, A. D. Leonard, B. K. Price, M. M. Cheng, P. Decuzzi, J. M. Tour, F. Robertson, M. Ferrari, *Nat. Nanotechnol.* **2008**, *3*, 151.

[29] M. Ferrari, *Trends Biotechnol.* **2010**, *28*, 181.

[30] P. Decuzzi, M. Ferrari, *Biomaterials* **2008**, *29*, 377.

[31] P. Decuzzi, B. Godin, T. Tanaka, S. Y. Lee, C. Chiappini, X. Liu, M. Ferrari, *J. Controlled Release* **2010**, *141*, 320.

[32] T. Tanaka, L. S. Mangala, P. E. Vivas-Mejia, R. Nieves-Alicea, A. P. Mann, E. Mora, H. D. Han, M. M. Shahzad, X. Liu, R. Bhavane, J. Gu, J. R. Fakhoury, C. Chiappini, C. Lu, K. Matsuo, B. Godin, R. L. Stone, A. M. Nick, G. Lopez-Berestein, A. K. Sood, M. Ferrari, *Cancer. Res.* **2010**, *70*, 3687.

[33] M. Ferrari, *Nat. Rev. Clin. Oncol.* **2010**, *7*, 485.

[34] J. You, G. Zhang, C. Li, *ACS Nano* **2010**, *4*, 1033.

[35] W. Lu, C. Xiong, G. Zhang, Q. Huang, R. Zhang, J. Z. Zhang, C. Li, *Clin. Cancer Res.* **2009**, *15*, 876.

[36] J. S. Ananta, B. Godin, R. Sethi, L. Moriggi, X. Liu, R. E. Serda, R. Krishnamurthy, R. Muthupillai, R. D. Bolskar, L. Helm, M. Ferrari, L. J. Wilson, P. Decuzzi, *Nat. Nanotechnol.* **2010**, *5*, 815.

[37] H. H. Richardson, M. T. Carlson, P. J. Tandler, P. Hernandez, A. O. Govorov, *Nano Lett.* **2009**, *9*, 1139.

[38] D. K. Roper, W. Ahn, M. Hoepfner, *J. Phys. Chem. C* **2007**, *111*, 3636.

[39] C. J. Huang, J. Dostalek, W. Knoll, *Biosens. Bioelectron.* **2010**, *26*, 1425.

[40] T. Jensen, L. Kelly, A. Lazarides, G. C. Schatz, *J. Cluster Sci.* **1999**, *10*, 295.

[41] S. A. Maier, P. G. Kik, H. A. Atwater, S. Meltzer, E. Harel, B. E. Koel, A. A. G. Requicha, *Nat. Mater.* **2003**, *2*, 229.

[42] W. Rechberger, A. Hohenau, A. Leitner, J. Krenn, B. Lamprecht, F. Aussenegg, *Opt. Commun.* **2003**, *220*, 137.

[43] A. O. Govorov, W. Zhang, T. Skeini, H. Richardson, J. Lee, N. A. Kotov, *Nanoscale Res. Lett.* **2006**, *1*, 84.

[44] H. Hövel, S. Fritz, A. Hilger, U. Kreibig, M. Vollmer, *Phys. Rev. B* **1993**, *48*, 18178.

[45] M. Hu, X. Wang, G. Hartland, V. Salgueiriño-Maceira, L. Liz-Marzán, *Chem. Phys. Lett.* **2003**, *372*, 767.